Role of fourth-order phase-space moments in collective modes of trapped Fermi gases

Silvia Chiacchiera
Centro de Física Computacional, Department of Physics, University of Coimbra, P-3004-516 Coimbra, Portugal

Thomas Lepers and Dany Davesne
Université de Lyon, F-69622 Lyon, France; Univ. Lyon 1, Villeurbanne; CNRS/IN2P3, UMR5822, IPNL

Michael Urban
Institut de Physique Nucléaire, CNRS/IN2P3 and Univ. Paris-Sud 11, 91406 Orsay cedex, France

(Dated: July 5, 2011)

We study the transition from hydrodynamic to collisionless behavior in collective modes of ultracold trapped Fermi gases. To that end, we solve the Boltzmann equation for the trapped Fermi gas via the moments method. We showed previously that it is necessary to go beyond second-order moments if one wants to reproduce the results of a numerical solution of the Boltzmann equation. Here, we will give the detailed description of the method including fourth-order moments. We apply this method to the case of realistic parameters, and compare the results for the radial quadrupole and scissors modes at unitarity to experimental data obtained by the Innsbruck group. It turns out that the inclusion of fourth-order moments clearly improves the agreement with the experimental data. In particular, the fourth-order moments reduce the effect of collisions and therefore partially compensate the effect of the enhanced in-medium cross section at low temperatures.

PACS numbers: 67.85.Lm,03.75.Ss

I. INTRODUCTION

The study of collective modes of trapped two-component Fermi gases revealed interesting information about different dynamical regimes [1]. Initially, the aim was to find signals for the superfluid-normal phase transition. However, near a Feshbach resonance, the atom-atom scattering cross section can be large enough to ensure (normal-fluid) hydrodynamic behavior of the gas above the superfluid critical temperature T_c. In this case, a change in the behavior of the gas is observed at much higher temperature, when the gas gets more and more dilute until the collisionless regime is reached. The most interesting modes in this context are those which in the collisionless case exhibit deformations in both coordinate and momentum space. Such modes are, e.g., the quadrupole and the scissors modes. In the presence of superfluidity or collisions, the deformation of the momentum sphere is suppressed, so that the frequencies of these modes are different from those in the collisionless case. In the intermediate regime, the damping of these modes is very strong. Both the radial quadrupole mode and the scissors mode were experimentally studied by the Innsbruck group [1–3].

From the theoretical side, the continuous transition from collisionally hydrodynamic to collisionless behavior can be studied by using the semiclassical Boltzmann equation. At present, there is no technique which would allow for a fully quantum mechanical description of collective modes of systems containing a few hundred thousand particles, including the collisional effects. But even the solution of the Boltzmann equation is far from being simple, and most of the time further approximations are made. A very common approximation is the relaxation-time approximation, which was used, together with the so-called scaling ansatz, to describe collective modes and the expansion of the gas after the trap is switched off [4]. In the case of collective modes, this method is equivalent to the method of phase-space moments up to second order, which was applied to the radial quadrupole, scissors, and breathing modes [3, 5, 6]. In both methods, the phase-space distribution function is constrained to a simple form, but the advantage is that one can perform computations almost analytically.

There are other approaches like the fully numerical solution of the Boltzmann equation as developed, e.g., in Refs. [7–10]. In this case no constraint is put on the functional form of the distribution function, but the price to pay is that the computations are very time consuming. Maybe the computation time could be significantly reduced by using new adaptive algorithms [11], but to our knowledge, no numerical calculation has been performed so far for degenerate Fermi gases with parameters (number of atoms, trap geometry) corresponding to real experiments.

In our previous work [9], we compared the results of a numerical simulation of the quadrupole mode in a spherical trap containing a reduced number of atoms with the corresponding results of the second-order moments method. The surprising outcome was that the second-order moments method strongly overestimates the effects of collisions. This problem could be cured to a large extent by generalizing the method of moments to fourth order. This is our main motivation for the present work, where we apply the fourth-order moments method to the radial quadrupole and scissors modes in a realistic trap

geometry, and compare it directly with the experimental results of Ref. [3].

The Boltzmann equation requires as microscopic input the mean-field potential (in the Vlasov part) and the cross section (in the collision integral). Here, the mean field will be neglected since we found in Ref. [6] that it affects only very weakly the frequencies and damping rates of the collective modes near unitarity. The main effect comes clearly from the collisions. In the case of large scattering length a and temperature slightly above T_c, one expects the Fermi gas to be in the "pseudogap regime" in which pair correlations play an important role although the pairs are not condensed. In this regime, the relaxation time is strongly reduced since the scattering cross section calculated in the surrounding medium is enhanced as compared with the free one [12] – an effect which in the context of nuclear physics has already been known for a couple of years [13]. Previous studies [3, 6] using the in-medium cross section in trapped Fermi gases found that this reduction of the relaxation time badly deteriorates the agreement with the experimental results. Here we argue that this discrepancy was, at least to some extent, due to the failure of the second-order moments method and not due to the enhancement of the in-medium cross section.

The paper is organized as follows. In Sec. II we describe the method, starting with a very general formulation and specializing then to the scissors and radial quadrupole modes. We explain how the response of the system is obtained and how we extract from it the frequencies and damping rates. In Sec. III we discuss our results. We show how the inclusion of fourth-order moments affects the response function and the corresponding frequencies and damping rates and compare the theoretical results with experimental data. In Sec. IV we summarize and give an outlook to future studies. Some technical details are given in the appendix.

Throughout the article, we use units with $\hbar = k_B = 1$.

II. FORMALISM

A. Moments method for the Boltzmann equation

We consider a two-component $(\uparrow,\downarrow)$ gas of Fermi atoms of mass m and with an interspecies attractive interaction (the scattering length is $a < 0$). The gas is loaded in a harmonic, usually anisotropic, trap

$$V(\mathbf{r}) = \frac{m}{2}(\omega_x^2 x^2 + \omega_y^2 y^2 + \omega_z^2 z^2) \; . \tag{1}$$

Moreover, since we are interested in collective modes and their time evolution, we include in the external potential felt by the atoms a small time-dependent part $\delta V(\mathbf{r}, t)$, that will be used to simulate the excitation of the mode. As mentioned before, the mean field felt by the atoms due to their interaction will be neglected here, since at unitarity it is only of minor importance for the properties of collective modes as compared with the effects coming from collisions between atoms [6].

In the normal fluid phase and under other assumptions we already discussed in Ref. [6], we can describe the system with a semiclassical distribution function $f_\sigma(\mathbf{r}, \mathbf{p}, t)$, where $\sigma = \uparrow, \downarrow$. We restrict ourselves to the case of an unpolarized gas ($N_\uparrow = N_\downarrow \equiv N/2$) and to excitations where the two components move together: $f_\uparrow = f_\downarrow \equiv f$. The normalization of f is[1]

$$\int \frac{d^3r d^3p}{(2\pi)^3} f(\mathbf{r}, \mathbf{p}, t) = \frac{N}{2} \tag{2}$$

and the average value of a generic quantity $\chi(\mathbf{r}, \mathbf{p})$ is

$$\langle \chi \rangle = \frac{2}{N} \int \frac{d^3r d^3p}{(2\pi)^3} f(\mathbf{r}, \mathbf{p}, t) \chi(\mathbf{r}, \mathbf{p}) \; . \tag{3}$$

In equilibrium, the distribution function reads

$$f_{eq}(\mathbf{r}, \mathbf{p}) = \frac{1}{e^{\beta[p^2/2m + V(\mathbf{r}) - \mu]} + 1} \, , \tag{4}$$

where $\beta = 1/T$ is the inverse of the temperature and μ is the chemical potential.

When the system is excited, the time evolution of f is governed by the Boltzmann equation [14]. We consider small perturbations δf of the distribution function from equilibrium and write them as

$$\delta f(\mathbf{r}, \mathbf{p}, t) = f_{eq}(\mathbf{r}, \mathbf{p})[1 - f_{eq}(\mathbf{r}, \mathbf{p})] \Phi(\mathbf{r}, \mathbf{p}, t) \, . \tag{5}$$

The function $\Phi(\mathbf{r}, \mathbf{p}, t)$ can be assumed to be smooth since the fact that δf is peaked near the Fermi surface is already accounted for by the prefactor $f_{eq}(1 - f_{eq})$. The linearized Boltzmann equation then reads

$$f_{eq}(1 - f_{eq}) \Big(\dot{\Phi} + \frac{\mathbf{p}}{m} \cdot \boldsymbol{\nabla}_r \Phi - \boldsymbol{\nabla}_r V \cdot \boldsymbol{\nabla}_p \Phi + \beta \frac{\mathbf{p}}{m} \cdot \boldsymbol{\nabla}_r \delta V \Big) = -I[\Phi] \, . \tag{6}$$

The linearized collision integral in the right-hand side is

$$I[\Phi] = \int \frac{d^3p_1}{(2\pi)^3} \int d\Omega \frac{d\sigma}{d\Omega} \frac{|\mathbf{p} - \mathbf{p}_1|}{m} f_{eq} f_{eq\,1} \times (1 - f'_{eq})(1 - f'_{eq\,1})(\Phi + \Phi_1 - \Phi' - \Phi'_1) \, . \tag{7}$$

The various f_{eq} and Φ are all evaluated at the same $\mathbf{r}, t$ but at different momenta $\mathbf{p}$, $\mathbf{p}_1$, $\mathbf{p}'$, or $\mathbf{p}'_1$, respectively, which due to momentum and energy conservation satisfy $\mathbf{p} + \mathbf{p}_1 = \mathbf{p}' + \mathbf{p}'_1 \equiv \mathbf{k}$ and $|\mathbf{p} - \mathbf{p}_1| = |\mathbf{p}' - \mathbf{p}'_1| \equiv 2q$. The solid angle between the initial and final relative momenta in the center-of-mass frame, $\mathbf{q}$ and $\mathbf{q}'$, is denoted Ω. The cross-section $d\sigma/d\Omega$ used in the present

[1] Notice that this normalization differs from that given in Ref. [6] by a factor $(2\pi)^3$.

paper is the in-medium cross section which is calculated as described in Ref. [6]. At temperatures close to the superfluid transition temperature T_c, this cross-section is strongly enhanced with respect to the free one $d\sigma_0/d\Omega = a^2/[1+(qa)^2]$, at least for collision partners near the Fermi surface with zero total momentum.

Since the function Φ is supposed to be smooth, one can try to approximate it by a polynomial in the components of $\mathbf{r}$ and $\mathbf{p}$ with time-dependent coefficients c_i,

$$\Phi(\mathbf{r},\mathbf{p},t) = \sum_{i=1}^{n} c_i(t)\phi_i(\mathbf{r},\mathbf{p}) \ . \tag{8}$$

The choice of the basis functions ϕ_i depends on the mode one wants to describe (see discussions in Refs. [6, 15]). However, let us first explain the general idea before focusing on the examples of the radial quadrupole and scissors modes.

In order to obtain the so-called response function, it is sufficient to consider a perturbation which is a δ pulse, i.e.,

$$\delta V(\mathbf{r},t) = \delta(t)\hat{V}(\mathbf{r}) \, . \tag{9}$$

Then the Fourier transform of Eq. (6) with respect to t gives

$$\sum_{i=1}^{n} c_i(\omega)\Big[f_{eq}(1-f_{eq})\Big(-i\omega\phi_i + \frac{\mathbf{p}}{m}\cdot\boldsymbol{\nabla}_r\phi_i - \boldsymbol{\nabla}_r V\cdot\boldsymbol{\nabla}_p\phi_i\Big) + I[\phi_i]\Big] = -f_{eq}(1-f_{eq})\beta\frac{\mathbf{p}}{m}\cdot\boldsymbol{\nabla}_r\hat{V}(\mathbf{r}) \, , \tag{10}$$

where $c_i(\omega)$ is the Fourier transform of $c_i(t)$. Now we take the moments of Eq. (10), i.e., we multiply it by each of the basis functions ϕ_i and integrate over phase space. In this way, we obtain n coupled linear algebraic equations for the n coefficients $c_i(\omega)$. In matrix form, they can be written as

$$\sum_{j=1}^{n} A_{ij}c_j(\omega) = a_i \, , \tag{11}$$

where

$$A_{ij} = -i\omega M_{ij} + A_{ij}^{trans} + A_{ij}^{coll} \, , \tag{12}$$

$$M_{ij} = \int \frac{d^3r d^3p}{(2\pi)^3} f_{eq}(1-f_{eq})\phi_i\phi_j \, , \tag{13}$$

$$A_{ij}^{trans} = \int \frac{d^3r d^3p}{(2\pi)^3} f_{eq}(1-f_{eq})\phi_i\Big\{\phi_j, \frac{p^2}{2m}+V\Big\} \, , \tag{14}$$

$$A_{ij}^{coll} = \int \frac{d^3r d^3p}{(2\pi)^3}\phi_i I[\phi_j] \, , \tag{15}$$

and

$$a_i = -\frac{\beta}{m}\int \frac{d^3r d^3p}{(2\pi)^3}\phi_i f_{eq}(1-f_{eq})\mathbf{p}\cdot\boldsymbol{\nabla}_r\hat{V}(\mathbf{r}) \, . \tag{16}$$

The contribution A_{ij}^{trans} of the transport part of the Boltzmann equation to A_{ij} has been written in a compact form using the Poisson brackets $\{\cdot,\cdot\}$. One can show that M and A^{coll} are symmetric matrices, while A^{trans} is antisymmetric.

Once we have solved Eq. (11) for the coefficients $c_i(\omega)$, we know the time-dependent distribution function $f_{eq} + \delta f$ and we can obtain the time evolution of the average of any dynamical quantity using Eq. (3).

In summary, making a polynomial ansatz for the time-dependent distribution function, we reduced the linearized Boltzmann equation from an integro-differential equation to a system of n coupled linear algebraic equations for the coefficients c_i.

B. Scissors and quadrupole modes

Consider an elongated trap with elliptic transverse section (i.e., $\omega_x > \omega_y \gg \omega_z$) containing a gas in equilibrium. The scissors mode is a collective mode that is excited by tilting the trap by a small angle ($\simeq 5°$) around the z-axis. After this excitation, the cloud is rotating back and forth around the z axis, and what is measured is the time dependence of the angle of the orientation of the oscillating cloud with respect to the trap potential. For the details on the experimental realization of this mode and the results at finite temperature and different scattering lengths, see Refs. [1, 3].

If the initial potential is harmonic, the scissors mode is excited by the perturbation

$$\hat{V}(\mathbf{r}) = \alpha\, xy \, , \tag{17}$$

where α is a factor characterizing the strength of the perturbation. Under the assumption that the shape of the cloud does not change during the oscillation, the measured angle is proportional to the expectation value

$$Q(t) = \langle xy \rangle \, . \tag{18}$$

The minimal ansatz for the function Φ that can reproduce the scissors mode contains four terms and reads [3, 5, 6]

$$\Phi_{2nd} = c_1 xy + c_2 p_x p_y + c_3 x p_y + c_4 y p_x \, . \tag{19}$$

All four terms are of second order in the components of $\mathbf{r}$ and $\mathbf{p}$. In fact, at second order, there are no other combinations which satisfy the symmetry of this excitation which is odd under $(x,p_x) \to (-x,-p_x)$, odd under $(y,p_y) \to (-y,-p_y)$, and even under $(z,p_z) \to (-z,-p_z)$. In the present case of a harmonic potential without mean field, this set of basis functions is closed with respect to the operators that are in the transport part of the Boltzmann equation, i.e., on the left-hand side of Eq. (6).

As noted in Ref. [9] in the case of the quadrupole mode in a spherical trap, the method of second-order moments

strongly overestimates the collisional effects because it implicitly neglects the position dependence of the relaxation time τ. Remember that the effect of collisions is to produce hydrodynamic behavior by maintaining the momentum distribution spherical. The deformation of the momentum distribution is described by the second term in Φ_{2nd}, i.e., the term $\propto p_x p_y$. So, the corresponding coefficient c_2 is large in the case of few or no collisions and small in the case of frequent collisions. In the trapped system, however, the collision rate is very different depending on the position: Near the center, the density and thus the collision rate is much higher than at the surface. Therefore, the deformation of the momentum distribution should depend on the position. This cannot be accomplished with the ansatz (19), since the term $\propto p_x p_y$ is independent of $\mathbf{r}$.

Let us therefore go to the next higher order, which is fourth order. At this order, terms like $x^2 p_x p_y$ etc. appear which allow us to describe the position dependence of the deformation of the momentum distribution. Keeping all terms which respect the symmetries mentioned above, we must then include 32 terms into the ansatz for Φ:

$$\Phi_{4th}(\mathbf{r},\mathbf{p},t) = \sum_{i=1}^{32} c_i(t)\phi_i(\mathbf{r},\mathbf{p})\,. \tag{20}$$

The basis functions ϕ_i can be compactly defined in the following way:

$$\phi_{i+4(j-1)}(\mathbf{r},\mathbf{p}) = g_i(\mathbf{r},\mathbf{p})h_j(\mathbf{r},\mathbf{p})\,, \tag{21}$$

where $i = 1,\ldots,4$ and $j = 1,\ldots,8$, and

$$\begin{aligned} g_1 &= xy\,, \quad g_2 = p_x p_y\,, \quad g_3 = x p_y\,, \quad g_4 = y p_x \\ h_1 &= 1\,, \quad h_2 = x^2\,, \quad h_3 = y^2\,, \quad h_4 = z^2 \\ h_5 &= p_x^2\,, \quad h_6 = p_y^2\,, \quad h_7 = p_z^2\,, \quad h_8 = z p_z\,. \end{aligned} \tag{22}$$

It is easily seen that the first four terms of Φ_{4th} reproduce Φ_{2nd}, while the subsequent ones are fourth-order terms in the components of $\mathbf{r}$ and $\mathbf{p}$.

Let us now turn to another mode, the radial quadrupole mode in an axially symmetric trap, $\omega_x = \omega_y$. In Refs. [3, 6], the corresponding perturbation was written as $\hat{V} \propto x^2 - y^2$ and the measured observable was $\langle x^2 - y^2\rangle$. However, since the trap is axially symmetric, we can rotate the coordinate system by 45° around the z axis without changing anything. By doing so, one sees immediately that the perturbation is then of the form $\hat{V} \propto xy$ and the measured observable becomes $\langle xy\rangle$, like for the scissors mode. In conclusion, the radial quadrupole mode is a special case of the scissors mode in the limit of equal trap frequencies $\omega_x = \omega_y$, and it therefore does not require any additional effort to describe both modes.

C. Response function

As already mentioned, we follow the observable $Q = \langle xy\rangle$, which, with our choice of basis functions, can be written as $Q = \langle\phi_1\rangle$. Using Eqs. (5) and (8), this expectation value can be expressed in terms of the coefficients c_i as

$$Q(\omega) = \frac{2}{N}\sum_{i=1}^{32} M_{1i}c_i(\omega)\,, \tag{23}$$

where M_{1i} are the elements of the first row of the matrix M defined in Eq. (13).

Also the vector a on the right-hand side of the linear system of equations (11) for the coefficients $c_i(\omega)$ can be expressed with the help of the matrix M. Note that $\mathbf{p}\cdot\boldsymbol{\nabla}_r\hat{V}(\mathbf{r}) = \alpha(xp_y + yp_x) = \alpha(\phi_3 + \phi_4)$, so that Eq. (16) becomes

$$a_i = -\frac{\alpha\beta}{m}(M_{i3} + M_{i4})\,. \tag{24}$$

Now, the linear system of equations (11) for the coefficients c_i has to be solved. After some algebra (see appendix), the result for the response function can be written as

$$Q(\omega) = \frac{-2i\alpha\beta}{Nm}\sum_{k=1}^{n}\frac{(MP)_{1k}[(P^{-1})_{k3} + (P^{-1})_{k4}]}{\omega - \omega_k + i\Gamma_k}\,, \tag{25}$$

where $\Gamma_k + i\omega_k$ is the kth eigenvalue of the matrix $M^{-1}(A^{trans} + A^{coll})$ and P is the matrix containing in its columns the corresponding eigenvectors.

It should be pointed out that it is a very tedious work to calculate the elements of the matrices M, A^{trans} and A^{coll} corresponding to the fourth-order moments. Here, we made use of the Mathematica software to derive the expressions. After that, the actual numerical calculations are quite fast, the only time-consuming part is the Monte-Carlo integration of the moments of the collision term in A^{coll}. The numerical inversion and diagonalization of a 4×4 (second-order method) or 32×32 (fourth-order method) matrix does not pose any problem. More details about the calculation of the matrices are given in the appendix.

For the discussion, the imaginary part of $Q(\omega)$ is particularly useful, since this so-called strength function describes the excitation spectrum corresponding to the mode under consideration.

D. Frequencies and damping rates

In the previous literature [3, 6], where the second-order moment method was used, the frequencies and damping rates of the collective modes were identified with the real and imaginary parts of the solutions of the characteristic equation $\det A = 0$. These are of course equal to the imaginary and real part of the eigenvalues of the matrix $M^{-1}(A^{trans} + A^{coll})$ mentioned above. Now, this method is not applicable any more. At fourth order, there are many eigenvalues, and sometimes they lie close to each

other and have comparable strength in the response function, so that it is not clear which one should be chosen.

The question arises what is the physical meaning of several poles if there is in reality only one damped collective mode. In order to get a better understanding of this question, let us have a look at a simpler example, namely a zero-sound wave in a uniform system. For this case, comparisons between the moments method up to very high order and exact solutions exist in the literature [16, 17]. In the zero-temperature case, it was found [16] that, with increasing order of the moments method, the distribution of sharp peaks in the response function (i.e., poles just below the real ω axis) converges to the continuous spectrum (i.e., a branch cut just below the real ω axis) of the exact solution of the Vlasov equation. Hence, in order to extract the Landau damping from the results of the moments method, one has to consider the distribution of eigenfrequencies rather than look at their imaginary parts. In the case of finite temperature [17], the collisions provide an additional damping mechanism and they lead to complex eigenfrequencies.

From the preceding discussion it is clear that the frequency and damping of a mode cannot be obtained from the real and imaginary parts of the individual eigenfrequencies given by the moments method, but that one has to consider the total response function. This point of view is confirmed by the good agreement between the response functions obtained by the fourth-order moments method and by numerical simulations in Ref. [9].

Besides this theoretical question, there is a more practical point one should consider. The idea is that we want to compare with experimental data, which were obtained by fitting the observed oscillation of the cloud with an exponentially damped cosine function. More precisely, in the case of the quadrupole mode, the observed oscillation is fitted with a function of the form [2]

$$Q_{fit}(t) = C_1 e^{-\Gamma t}\cos(\omega t + \varphi) + C_2 e^{-\kappa t}\,, \qquad (26)$$

while in the case of the scissors mode, the oscillation is either fitted with

$$Q_{fit}^{low\text{-}T}(t) = C e^{-\Gamma t}\cos(\omega t + \varphi) \qquad (27)$$

at low temperature (hydrodynamic regime), or with

$$Q_{fit}^{high\text{-}T}(t) = \sum_{k=1}^{2} C_k e^{-\Gamma_k t}\cos(\omega_k t + \varphi_k) \qquad (28)$$

at high temperature (collisionless regime) [1]. So, we will determine the frequency and damping rate corresponding to our response function $Q(\omega)$ by fitting it with Eq. (26) in the case of the quadrupole mode and with Eq. (27) or (28) in the case of the scissors mode. In the case of a fit with two frequencies, we concentrate on the mode with the higher frequency.

TABLE I: Trap parameters of the Innsbruck experiments. Both experiments were done with 600 000 atoms of ^{6}Li in the unitary limit ($1/k_F a = 0$) [3].

mode	$\omega_x/2\pi$ (Hz)	$\omega_y/2\pi$ (Hz)	$\omega_z/2\pi$ (Hz)
scissors	1600	700	30
quadrupole	1800	1800	32

III. RESULTS

A. Scissors and quadrupole strength functions

In Fig. 1 we plot the results for $\mathrm{Im}\,Q(\omega)$ obtained at second and fourth order for the scissors and quadrupole modes at unitarity. The parameters of the trap and the number of ^{6}Li atoms are chosen as in Ref. [3], so that a comparison with the experimental data is possible, see Table I. In the upper panels of Fig. 1, the scissors response is plotted at various temperatures ($T/T_F = 0.4,\ 0.6,\ 0.8$). Since mean-field effects are not taken into account, the limiting frequencies for the scissors mode in the hydrodynamic and collisionless regimes are $\omega_{S,hd} = \sqrt{\omega_x^2 + \omega_y^2}$ and $\omega_{S,cl\pm} = \omega_x \pm \omega_y$, respectively [18]. (In the collisionless regime, two different modes can be excited.) In the trap under consideration, these frequencies are $\omega_{S,hd} \simeq 1.65\ \omega_r$, $\omega_{S,cl-} \simeq 0.85\ \omega_r$, and $\omega_{S,cl+} \simeq 2.17\,\omega_r$, where $\omega_r = \sqrt{\omega_x\omega_y}$ is the average radial frequency. Let us first analyse the second-order (dashed) curves. At $T/T_F = 0.4$, the response is peaked almost at $\omega_{S,hd}$: we are in the hydrodynamic regime. As the temperature increases, the peak becomes broader (strong damping) and gets shifted towards the higher frequency $\omega_{S,cl+}$. At second order, the lower mode at $\omega_{S,cl-}$ is not yet visible at $T/T_F = 0.8$ since it is still too strongly damped. The fourth-order results (full lines) deviate more and more from the lowest order ones as the temperature increases. The most striking feature is that the shape itself of the response function is modified by the inclusion of the higher-order moments. We also observe that at fourth order the lower peak at $\omega_{S,cl-}$ is already clearly visible at $T/T_F = 0.8$.

In the second row of Fig. 1, we plot the results for the quadrupole mode. The limiting frequencies of this mode in the hydrodynamic and collisionless limits are $\omega_{Q,hd} = \sqrt{2}\omega_r$ and $\omega_{Q,cl} = 2\omega_r$, respectively (again without mean-field). The second order (dashed) results show how the peak moves from the hydrodynamic to the collisionless limit as the temperature increases. Consider now the fourth-order (full) lines. At $T/T_F = 0.4$ and $T/T_F = 0.8$ the response shows a clear peak, whose position is however displaced towards higher frequencies, as compared to the second-order results. At $T/T_F = 0.6$, the shape of the peak itself is deformed, but again its centroid is moved towards higher frequencies. This is in qualitative agreement with our finding in Ref. [9] that the second-order moments method overestimates the col-

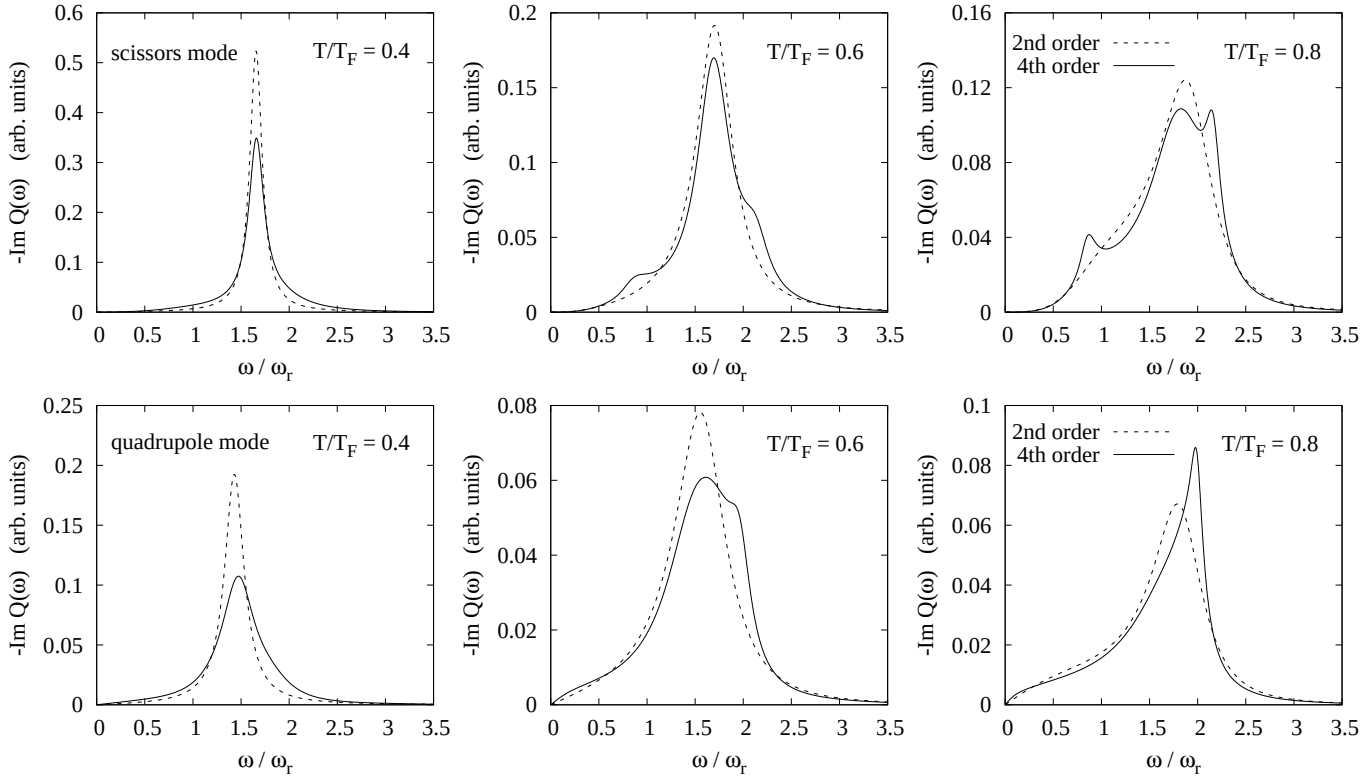

FIG. 1: The imaginary part of the scissors (first row) and quadrupole (second row) response function as function of the frequency at temperatures $T/T_F = 0.4$, 0.6, 0.8 (from left to right). The dashed lines represent the second-order results, the full ones the fourth-order results. The frequency is in units of the radial trap frequency $\omega_r = \sqrt{\omega_x \omega_y}$. The trap parameters are listed in Table I.

lisional effects, i.e., the second-order result is always too close to the hydrodynamic limit.

B. Frequencies and damping rates

In order to make a quantitative comparison of our results with the data, we extract from $Q(\omega)$ the frequency and damping of the mode by fitting the response function as explained in Sec. II D. The results are shown in Fig. 2. Let us first look at the results for the scissors mode (first row). Because of the two different fits at low and high temperatures (using one or two damped cosine functions), there are two curves for each method (second and fourth order moments). In the range of T/T_F between 0.7 and 0.8 we plot both curves in order to show the dependence on the fit. For $T/T_F > 0.8$, the gas is closer to the collisionless regime where two modes are present, and we keep only the fit with two damped cosine functions. For $T/T_F < 0.7$, we show only the fit with a single damped cosine function. Let us now compare the results obtained with the second-order (dashed lines) and fourth-order (solid lines) moments methods. The most important difference is that the transition from low frequency (hydrodynamic regime) to high frequency (collisionless regime) is shifted to lower temperature by the inclusion of fourth-order moments. This was to be expected since, as we discussed above, the second-order moments method overestimates the collisional effects. Therefore, for temperatures below $0.9T_F$, the fourth-order frequencies are in better agreement with the data than the second-order ones. Only at high temperatures, it seems that the second-order frequency, which approaches the limiting value $\omega_{S,cl+}$ much more slowly, is in better agreement with the data. Concerning the damping, there is quite a big difference between the second- and fourth-order results, but it is not really clear whether the fourth-order represents an improvement or not.

The improvement due to the fourth-order moments is more clearly seen in the results for the quadrupole mode (second row of Fig. 2). Again, if the fourth-order moments are included, the transition from the hydrodynamic to the collisionless regime happens at lower temperatures, which greatly improves the agreement of both frequencies and damping rates with the data. But the difference between second- and fourth-order calculations does not only concern the temperature dependence. This can clearly be seen in the right figure, showing the damping as function of frequency, so that the temperature drops out. In this representation, the curve obtained with the fourth-order moments almost passes through the error bars of the data, which was by far not the case for

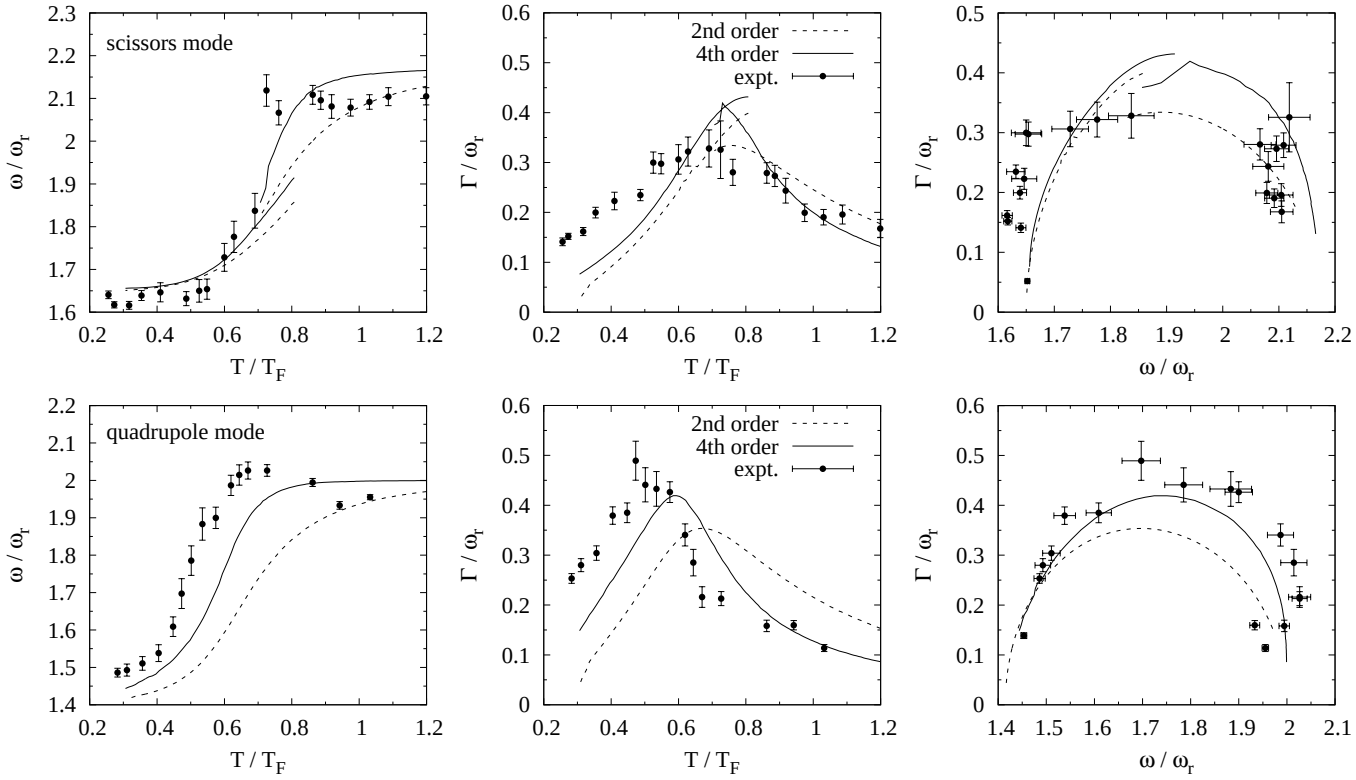

FIG. 2: Frequency (left) and damping rate (middle) of the scissors (first row) and radial quadrupole modes (second row) as functions of temperature as well as the representation damping vs. frequency (right) which is independent of possible uncertainties in the temperature measurement. The points with error bars are the experimental data from Ref. [3], the dashed lines are the second-order results, and the solid lines are fourth-order results. The trap parameters are listed in Table I.

the second-order results.

IV. SUMMARY AND CONCLUSIONS

In this work, we determined approximate solutions of the linearized Boltzmann equation for collective modes of trapped Fermi gases by using the method of phase-space moments. Here, we concentrated on the radial quadrupole and scissors modes. Contrary to previous literature [3, 5, 6], we did not only include the lowest (second) order moments which are necessary to describe the modes, but also the next (fourth) order. A comparison with a numerical solution of the Boltzmann equation [9] showed that the fourth order catches already the most important effects missed at second order, e.g., the position dependence of the Fermi-surface deformation. We therefore decided to apply this method to realistic cases in order to be able to compare with experimental data.

We showed that, if one includes higher than second-order moments, the shape of the response function does no longer resemble a single Lorentzian. Therefore, if one wants to extract the frequency and damping rate of a mode, the result depends on the ansatz for the fit function which is used. Our determination of these quantities is inspired by the procedure used by the experimentalists.

In the actual calculation of the moments of the collision term, A^{coll}, we used the in-medium cross section as defined in Ref. [6]. In previous works [3, 6] it was found that the in-medium enhancement of the cross section strongly deteriorates the agreement with the experimental results. This conclusion was, however, based on calculations using only second-order moments. Since the fourth-order contributions reduce the effect of collisions, the effect of the enhanced cross section is partially compensated. In fact, our new results, including the in-medium cross section and fourth-order moments, are in reasonable agreement with the data.

Another application of higher-order moments will be to quantify the effects of the anharmonicity of the trap potential, including also the mean field. Work in this direction is in progress. This might be helpful, e.g., for understanding the behavior of the frequencies and damping rates at high temperature (note that in Ref. [3] the experimental frequencies have been roughly corrected for anharmonicity effects by dividing them by the measured frequencies of the sloshing mode). For a detailed comparison with the experiment, however, many other effects should be accounted for, too. For instance, the measured quantity is not the response to a δ pulse, but the relaxation after the system was adiabatically deformed and then suddenly released at $t = 0$. This results, roughly

speaking, in an additional factor $1/\omega$ in the Fourier transform of the response of the system which can have some effect on the fitted frequency and damping rate. In addition, the observable measured in the experiment is not simply proportional to $\langle xy \rangle$, but depends also on the distribution in momentum space since the density profile in the xy plane is measured after an expansion. Without any doubt, it would be desirable to make a complete numerical simulation of the experiment, including the expansion phase.

Acknowledgments

S.C. is supported by FCT (Portugal) under the project SFRH/BPD/64405/2009.

Appendix A: Computation of A_{ij}

In this appendix we give some details about the computation of the matrix A defined in Eq. (12) and on its final form.

As in our practical calculations, we will use trap units, i.e., all quantities are made dimensionless by rescaling them by appropriate combinations of the atom mass m, the average trap frequency $\bar{\omega} = (\omega_x \omega_y \omega_z)^{1/3}$, the harmonic oscillator length $l_{ho} = 1/\sqrt{m\bar{\omega}}$ etc.

The matrix M

In order to compute M_{ij} defined in Eq. (13), it is convenient to define six-dimensional hyperspherical coordinates. To do this, we must first pass to isotropic spatial coordinates, and then to dimensionless ones, so that the $\mathbf{r}$ and $\mathbf{p}$ components can be treated together. We define

$$\begin{aligned} x &= l_{ho}(\bar{\omega}/\omega_x) X \cos\vartheta_1 \\ y &= l_{ho}(\bar{\omega}/\omega_y) X \sin\vartheta_1 \cos\vartheta_2 \\ z &= l_{ho}(\bar{\omega}/\omega_z) X \sin\vartheta_1 \sin\vartheta_2 \cos\vartheta_3 \\ p_x &= (1/l_{ho}) X \sin\vartheta_1 \sin\vartheta_2 \sin\vartheta_3 \cos\vartheta_4 \\ p_y &= (1/l_{ho}) X \sin\vartheta_1 \sin\vartheta_2 \sin\vartheta_3 \sin\vartheta_4 \cos\varphi \\ p_z &= (1/l_{ho}) X \sin\vartheta_1 \sin\vartheta_2 \sin\vartheta_3 \sin\vartheta_4 \sin\varphi \,. \end{aligned} \tag{A1}$$

The volume element becomes $d^3r d^3p = X^5 dX d\Omega_5$, and its angular part is

$$d\Omega_5 = \sin^4\vartheta_1 \sin^3\vartheta_2 \sin^2\vartheta_3 \sin\vartheta_4 d\vartheta_1 d\vartheta_2 d\vartheta_3 d\vartheta_4 d\varphi \,. \tag{A2}$$

The integration range is $[0, \infty[$ for X, $[0, 2\pi]$ for φ and $[0, \pi]$ for the ϑ_i. In these coordinates, the equilibrium distribution function reduces to

$$f_{eq}(X) = \frac{1}{e^{\beta(\bar{\omega}X^2/2 - \mu)} + 1} \,, \tag{A3}$$

and one obtains the useful relation

$$\frac{df_{eq}(X)}{dX} = -f_{eq}(1 - f_{eq})\beta\bar{\omega}X \,. \tag{A4}$$

Using the latter, one can check that

$$\int d\Omega_5 \int_0^\infty \frac{dX}{(2\pi)^3} X^5 f_{eq}(1 - f_{eq}) X^n = \frac{n+4}{\beta\bar{\omega}} \frac{N}{2} \langle X^{n-2} \rangle_{eq} \,. \tag{A5}$$

Then, it can easily be seen that the elements of M are proportional to $\langle X^n \rangle_{eq}$, $n = 2, 4, 6$. We choose to express them in terms of $\langle x^n \rangle_{eq}$: in trap units, the factors of proportionality contain the factor N/β, rational numbers and ratios of powers of the trap frequencies.

The matrix A^{trans}

Notice that in the case of a harmonic trap, the set $\{\phi_i\}$ is closed with respect to the operators in the left-hand side of Eq. (6), therefore one can find a matrix B of coefficients such that

$$\{\phi_j, \frac{p^2}{2m} + V\} = \sum_{k=1}^{n} \phi_k B_{kj} \,. \tag{A6}$$

Then, it is clear that the matrix A^{trans} defined in Eq. (14) can be written as a matrix product

$$A^{trans} = MB \,, \tag{A7}$$

where M denotes the matrix calculated in the preceding subsection.

The computation of the matrix B is straight-forward. In trap units, its elements are simply given by powers of the trap frequencies multiplied by integer numbers.

The matrix A^{coll}

To compute the matrix elements A_{ij}^{coll}, that by definition are

$$\begin{aligned} A_{ij}^{coll} = \int \frac{d^3r d^3p}{(2\pi)^3} \phi_i(\mathbf{r}, \mathbf{p}) \int \frac{d^3p_1}{(2\pi)^3} \int d\Omega \frac{d\sigma}{d\Omega} \frac{|\mathbf{p} - \mathbf{p}_1|}{m} \\ \times f_{eq} f_{eq\,1} (1 - f'_{eq})(1 - f'_{eq\,1}) \Delta_{coll}[\phi_j] \,, \end{aligned} \tag{A8}$$

we follow the method outlined in Refs. [6, 19]. In the last equation we have used the compact notation $\Delta_{coll}[\phi] = \phi(\mathbf{r}, \mathbf{p}) + \phi(\mathbf{r}, \mathbf{p}_1) - \phi(\mathbf{r}, \mathbf{p}') - \phi(\mathbf{r}, \mathbf{p}'_1)$. To reduce the number of integrals in Eq. (A8), we define the variables $\mathbf{k} = \mathbf{p} + \mathbf{p}_1$, $\mathbf{q} = (\mathbf{p} - \mathbf{p}_1)/2$ and $\mathbf{q}' = (\mathbf{p}' - \mathbf{p}'_1)/2$ (remember that energy and momentum conservation imply $|\mathbf{q}| = |\mathbf{q}'|$). In these variables, one can write

$$\begin{aligned} f_{eq} f_{eq\,1} (1 - f'_{eq})(1 - f'_{eq\,1}) = \\ \frac{1}{4} \frac{1}{\cosh\beta(E - \mu) + \cosh\beta\mathbf{k} \cdot \mathbf{q}/2m} \\ \times \frac{1}{\cosh\beta(E - \mu) + \cosh\beta\mathbf{k} \cdot \mathbf{q}'/2m} \,, \end{aligned} \tag{A9}$$

with $E = k^2/8m + q^2/2m + V$. The factor $\phi_i \Delta[\phi_j]$ has to be computed and rewritten, as the rest of the integrand, in these variables, too. Then, we define a rotation that brings $\mathbf{k}$ (identified by the angles θ, φ) to be parallel to the z-axis in momentum space. We define R the matrix associated to such a rotation and apply it to all momenta: the old coordinates are related to the new ones by $(p_x, p_y, p_z) = R^{-1}(p_a, p_b, p_c)$, and in particular $(k_a, k_b, k_c) = (0, 0, k)$. Now the integration over θ, φ can be performed analytically, since all the dependence upon these variables is in the numerator of the integrand. We have thus reduced the number of integrals from eleven to nine. Next one defines spherical coordinates for $\mathbf{q}$ and $\mathbf{q}'$: their zenith and azimuth angles are θ_c, φ_c and θ'_c, φ'_c respectively. Since the dependence upon φ, φ'_c is only in the numerator, we can easily integrate over these variables, reducing the integral to a seven-dimensional one. Finally, the definition of scaled spatial coordinates $\tilde{r}_i \equiv \frac{\omega_i}{\bar{\omega}} r_i$ renders the trap potential, and therefore the integrand, spherically symmetric in the spatial coordinates: the integral is reduced to a five-dimensional one. As a result, the elements of A^{coll} are proportional, through rational numbers and ratios of powers of trap frequencies, to terms of the same type of the inverse relaxation time $1/\tau$ defined in Ref. [6]. More precisely, now there are twelve different terms of this type which are of the form

$$J_i = \frac{1}{20\pi^2 m} \int_0^\infty d\tilde{r}\, \tilde{r}^2 dk\, k^2 dq\, q^7 \frac{d\sigma}{d\Omega} \int_{-1}^{1} d\gamma d\gamma' F_i \times \frac{1}{\cosh\beta(E-\mu) + \cosh\beta k q \gamma/2m} \times \frac{1}{\cosh\beta(E-\mu) + \cosh\beta k q \gamma'/2m}\,, \quad \text{(A10)}$$

$i = 1, \ldots, 12$, where $E = k^2/8m + q^2/2m + m\bar{\omega}^2\tilde{r}^2/2$, $\gamma = \cos\theta_c$ and $\gamma' = \cos\theta'_c$. The factors F_i are polynomials of $\tilde{r}^2$, k^2, q^2, γ^2, and γ'^2. In particular, $F_1 = 1 + 2\gamma^2 - 3\gamma^2\gamma'^2$, such that J_1 is identical to I_S given in Eq. (B4) of Ref. [6], and is in fact the only non-zero term of A^{coll} at second order. The coefficients J_i are obtained numerically via a Monte Carlo integration and used to build A^{coll}.

Appendix B: Calculation of the response function

In this appendix we describe how the Fourier spectrum of a generic observable $\langle\chi\rangle$ after a generic perturbation $\hat{V}$ can be obtained.

First, one has to calculate the vector a_i defined in Eq. (16) [which is simple in the case $\hat{V} = xy$, cf. Eq. (24)]. Then, one has to express the expectation value of χ in terms of the coefficients c_i. Supposing that $\langle\chi\rangle_{eq} = 0$, the expectation value must be proportional to the c_i and one can thus write

$$\langle\chi\rangle = \sum_{i=1}^{n} b_i c_i = b^T c\,, \quad \text{(B1)}$$

where we changed to vector notation in the second equality, b and c being vectors with components b_i and c_i, respectively.

Inverting Eq. (11), one obtains

$$\begin{aligned}\langle\chi\rangle(\omega) &= b^T(-i\omega M + A^{trans} + A^{coll})^{-1} a \\ &= b^T[-i\omega \mathbb{1} + M^{-1}(A^{trans} + A^{coll})]^{-1} M^{-1} a\,.\end{aligned} \quad \text{(B2)}$$

Notice that M, A^{trans}, and A^{coll} are real matrices which are independent of ω. Now we perform the diagonalization

$$M^{-1}(A^{trans} + A^{coll}) = PDP^{-1}\,, \quad \text{(B3)}$$

with $D = \mathrm{diag}(\lambda_1, \ldots, \lambda_n)$. Since the original matrix is real, its eigenvalues λ_k are either real or they appear as complex conjugate pairs. If we identify the real and imaginary parts of the eigenvalues as $\lambda_k = \Gamma_k + i\omega_k$, we obtain

$$\begin{aligned}\langle\chi\rangle(\omega) &= b^T P(-i\omega\mathbb{1} + D)^{-1} P^{-1} M^{-1} a \\ &= i\sum_{k=1}^{n} \frac{(b^T P)_k (P^{-1} M^{-1} a)_k}{\omega - \omega_k + i\Gamma_k}\,.\end{aligned} \quad \text{(B4)}$$

This reduces to Eq. (25) in the special case $\hat{V} = \chi = xy$.

[1] M.J. Wright, S. Riedl, A. Altmeyer, C. Kohstall, E.R. Sánchez Guajardo, J. Hecker Denschlag, and R. Grimm, Phys. Rev. Lett. **99**, 150403 (2007).

[2] A. Altmeyer, S. Riedl, M.J. Wright, C. Kohstall, J. Hecker Denschlag, and R. Grimm, Phys. Rev. A **76**, 033610 (2007).

[3] S. Riedl, E.R. Sánchez Guajardo, C. Kohstall, A. Altmeyer, M.J. Wright, J. Hecker Denschlag, R. Grimm, G.M. Bruun, and H. Smith, Phys. Rev. A **78**, 053609 (2008).

[4] P. Pedri, D. Guéry-Odelin, and S. Stringari, Phys. Rev. A **68** 043608 (2003).

[5] G.M. Bruun and H. Smith, Phys. Rev. A **76**, 045602 (2007).

[6] S. Chiacchiera, T. Lepers, D. Davesne and M. Urban, Phys. Rev. A **79**, 033613 (2009).

[7] F. Toschi, P. Vignolo, S. Succi, and M.P. Tosi, Phys. Rev. A **67**, 041605(R) (2003).

[8] F. Toschi, P. Capuzzi, S. Succi, P. Vignolo, and M.P. Tosi, J. Phys. B **37**, S91 (2004).

[9] T. Lepers, D.Davesne, S.Chiacchiera and M. Urban Phys. Rev. A **82**, 023609 (2010).

[10] O. Goulko, F. Chevy, C. Lobo, preprint arXiv:1106.5773 (2011).

[11] A.C.J. Wade, D. Baillie, and P.B. Blakie, preprint arXiv:1105:2340 (2011).
[12] G.M. Bruun and H. Smith, Phys. Rev. A **72**, 043605 (2005).
[13] T. Alm, G. Röpke, and M. Schmidt, Phys. Rev. C **50**, 31 (1994).
[14] E.M. Lifshitz and L.P. Pitaevskii, *Physical Kinetics*, L.D. Landau and E.M. Lifshitz Course of Theoretical Physics Vol. 10 (Pergamon, Oxford, 1980).
[15] U. Al Khawaja, C.J. Pethick, and H. Smith, J. Low Temp. Phys. **118**, 127 (2000).
[16] J.P. da Providência, Nucl. Phys. A **489**, 111 (1988).
[17] S. Watabe, A. Osawa, and T. Nikuni, J. Low. Temp. Phys. **158**, 773 (2010).
[18] D. Guéry-Odelin and S. Stringari, Phys. Rev. Lett. **83**, 4452 (1999).
[19] L. Vichi, J. Low Temp. Phys. **121**, 177 (2000).